From Rings to Belts: Radiation-Assisted Growth of Dyson Swarms

Hao Ke

Independent researcher

Correspondence: Hao Ke, i@kehao.me

Manuscript revision: 15 October 2026

Abstract

Incremental Dyson-swarm construction requires configurations that accommodate additional collecting area. This paper constructs a sequence of finite-area latitude belts while retaining earlier nominal trajectories and prescribed attitudes. Established ideal-specular solar-sail dynamics supplies circular support states at a common stellar distance. The known minimum-lightness envelope sets the latitude interval for unchanged hardware. Within this limit, a reserved lattice keeps finite reflectors separated and direct stellar rays unobstructed at every relative row phase, including rays from a finite stellar emitting region. Solid-angle bounds show that direct first-pass interception from a central isotropic point source increases with each addition. A solar example assuming a total system areal density of 30 g per square metre extends from an equatorial ring to one degree north and south, intercepting approximately 0.149 per cent of stellar luminosity. Its hardware permits ideal support to 1.158 degrees; the lattice reserves only one degree. These results establish compatible nominal stages under independent-force assumptions. Insertion, stability, useful power and engineering feasibility remain unresolved.

Keywords: Dyson swarm; Solar sail; Radiation pressure; Displaced non-Keplerian orbit; Incremental construction

1. Introduction

A Dyson swarm need not be completed before its first elements operate. Incremental growth raises a geometric question: can new collecting area be added while earlier elements retain their assigned nominal motion? Dyson's energy-collection argument and subsequent classifications allow many distributed arrangements [1,2]. This paper examines one such arrangement: latitude rows supported by radiation pressure and orbital motion.

The ingredients of this architecture have precedents. Photovoltaic lightsails feature in Dyson Dots [3]. The Yuti transit simulator adds panels along latitude circles to illustrate a partially constructed swarm, while noting the dynamical difficulty of its non-equatorial configuration [4]. Displaced solar-sail orbit families and their minimum-lightness optimisation are established [5–7]. McInnes has proposed parallel displaced orbital planes for Dyson-swarm elements [8]. Relative motion and formation flying around displaced solar orbits have also been studied [9]. These precedents supply the construction geometry and local support theory used here.

Admissible single-element orbits must also fit together. Rows at different latitudes may rotate at different rates, so the arrangement must keep finite reflectors separated and direct stellar rays unobstructed at every relative phase. These requirements connect local force balance to the geometry of a growing population.

This paper supplies an explicit finite-area construction connecting an equatorial ring to successive latitude belts. A reserved lattice preserves separation and direct illumination at every relative row phase as finite reflectors are added individually. Each addition increases direct first-pass interception from a central isotropic source. Under the independent-force assumptions, earlier nominal trajectories and prescribed attitudes can then be retained. The inherited support envelope bounds the latitude interval for unchanged hardware; the new result is the joint compatibility construction. A solar example illustrates it through a sparse one-degree belt. The sequence describes configurations after placement; actual insertion and stable operation require separate analysis.

2. A Progressive Latitude-Belt Architecture

2.1 Geometry and the addition rule

All element centres lie at a common star-centred distance r. A chosen reference plane defines latitude ϕ, cylindrical radius $\rho = r\cos\phi$ and axial displacement $z = r\sin\phi$. The reference plane is a geometric choice in the central-field model; it need not coincide with the stellar equator. A latitude row is a population of independent elements following the same displaced circular path. It is not a mechanically connected ring.

Assign row j the latitude $\phi_j = j\,\delta$, angular rate ω_j and N equally spaced phase slots.

Stage J contains all occupied slots with $|j| \le J$. Increasing J adds new northern and southern rows while retaining every earlier trajectory and its prescribed sail attitude.

Fig. 1 shows these stages before hardware and collecting areas are specified. Its labelled half-width Φ marks the outermost row. Rows may rotate at different angular rates.

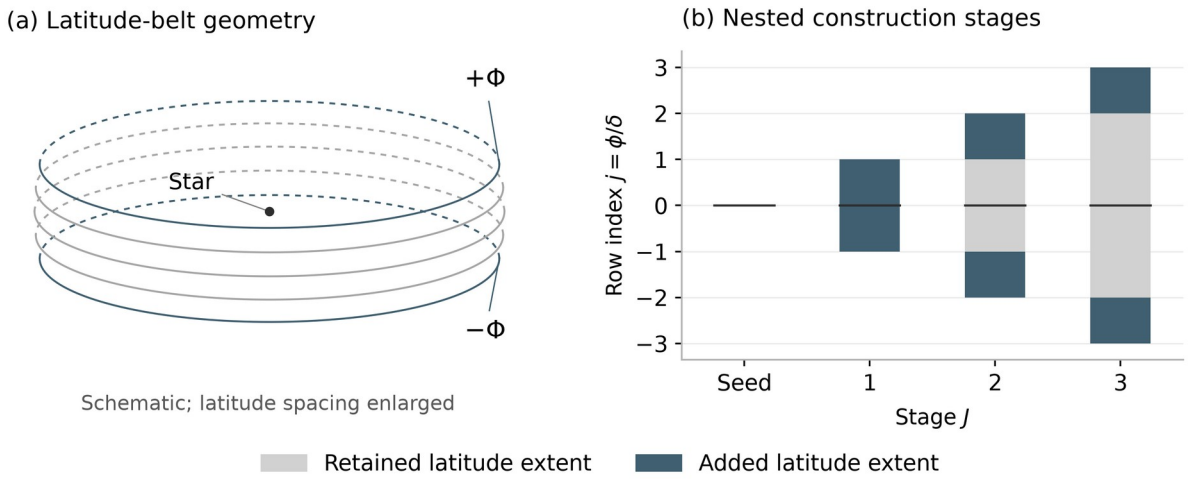


Fig. 1. Progressive latitude-belt architecture. Panel (a) enlarges the latitude spacing to show retained inner rows and new outer rows. Panel (b) illustrates nested stages with row indices rather than physical angles. Grey marks retained extent and dark shading marks additions; shading does not imply a continuous filled surface.

The centre of slot m follows

$$q_{jm}(t) = r\left(\cos\phi_j \cos\vartheta_{jm}, \cos\phi_j \sin\vartheta_{jm}, \sin\phi_j\right),$$

$$\vartheta_{jm} = \omega_j t + 2\pi m / N + \theta_j, m = 0, \ldots, N-1.$$

Here θ_j sets the initial phase of the row. Within a new row, elements may occupy previously reserved empty slots individually. Every partial subset inherits the separation properties of the completed slot pattern.

2.2 Elements and model assumptions

Each element is contained in a ball of radius a about its assigned centre. Its reflecting surface is a flat circular disc of radius a. The bound accommodates the disc's orientation; structural deformation is omitted. The support calculation applies the ideal specular-sail force at the disc centre with a prescribed attitude.

The model treats forces, visibility and interception separately. Centre dynamics uses point-source inverse-square gravity and radiation pressure; the

intercepted luminosity fraction also refers to a central isotropic point source. For direct visibility, the emitting region may fill a stellar ball of radius $R<r$. This finite radius enters only the occultation geometry. Extended-source radiation-pressure models can change sail forces, especially near the star [10,11]. The present force model omits those corrections, finite-aperture variations, mutual gravity and secondary reflected-light forces.

Each growth stage describes the configuration after placement. Transfers into reserved slots and the control needed to track the prescribed attitudes lie outside the model. Under the independent-force assumptions, adding an independently illuminated element leaves earlier force laws unchanged.

Two bounds govern the resulting sequence. Within the ideal constant-latitude family, the hardware sets the greatest supported latitude; the reserved lattice sets the belt half-width over which spacing and direct visibility are guaranteed.

3. Radiation-Assisted Support and Hardware Limits

3.1 Local dynamics

Radiation pressure permits a circular trajectory in a plane displaced from the star. At $z=constant\neq 0$, the sail's axial force balances axial gravity. The remaining inward cylindrical force supplies the centripetal acceleration. Fig. 2 defines the meridional geometry with enlarged illustrative angles.

The ideal specular-sail force law and displaced-orbit family follow established work [6,7], expressed here in latitude and cone-angle coordinates. Let $\mu=GM_{\star}$ and let γ denote the cone angle between the outward star-element line and the reflector normal in the meridional plane. Define

$$\beta=\frac{\sigma^{*}}{\sigma_{sys}},\sigma^{*}=\frac{L_{\star}}{2\pi GM_{\star}c},\nu=\frac{\omega}{\sqrt{\mu/r^{3}}}.$$

Here $L_{\star}$ and $M_{\star}$ denote stellar luminosity and mass, G is the gravitational constant and c is the speed of light. The quantity σ_{sys} is all supported system mass divided by physical reflector area. It is not the membrane areal density alone. The lightness number β references the face-on ideal-reflector force; the actual acceleration magnitude is $(\mu/r^{2})\beta\cos^{2}\gamma$. The quantity ν is an angular-rate ratio rather than a global fraction of gravity supported.

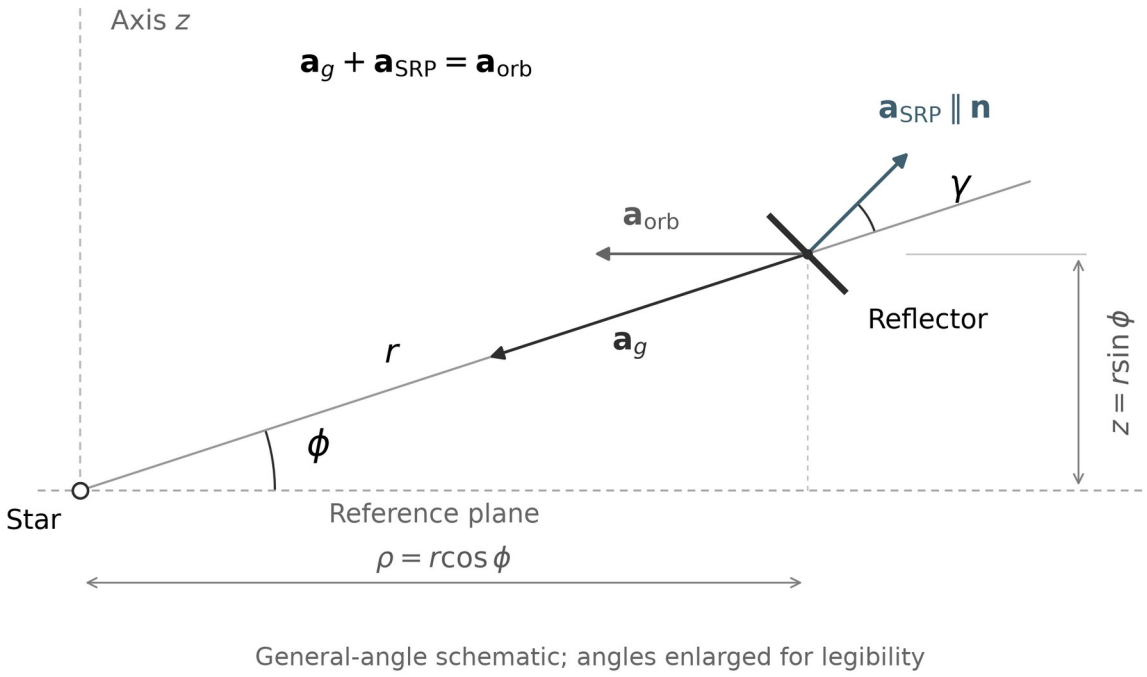


Fig. 2. General meridional force balance. Latitude ϕ is measured from the reference plane; sail cone angle γ is measured from the outward star-element line. Solar radiation pressure (SRP) acts along the reflector normal. Angles are enlarged for legibility and do not depict the one-degree example.

For the northern hemisphere the two force-balance equations are

$$\beta\cos^2\gamma\sin(\gamma+\phi)=\sin\phi,$$

$$\beta\cos^2\gamma\cos(\gamma+\phi)=\cos\phi(1-v^2).$$

Thus, for $0<\phi<\pi/2$,

$$\beta(\phi,\gamma)=\frac{\sin\phi}{\cos^2\gamma\sin(\gamma+\phi)},\ v^2=1-\tan\phi\cot(\gamma+\phi).$$

The restricted outward-thrust family uses $0\le\gamma\le\pi/2-\phi$. The southern states follow by reflecting the position and sail normal across the reference plane.

The equatorial seed must be treated separately. For unchanged hardware of lightness $0<\beta_0<1$, a radial-facing sail has $\gamma=0$ and $v=\sqrt{1-\beta_0}$. This finite-mass seed differs from the zero-lightness limit of the optimised envelope because its hardware is fixed. At nonzero latitude the normal rotates azimuthally with its row and must therefore be tracked.

3.2 Fixed-hardware continuation and support envelope

Unchanged hardware follows a continuous family only up to a finite latitude. The minimum required lightness $\beta_{cone,min}(\phi)$ is the latitude parametrisation of

McInnes's optimal halo mode [5, sec. 4.5]. Appendix B makes the algebraic correspondence explicit. Within the stated ideal sail family the optimum occurs at

$$\tan\gamma_* = \frac{2}{\sqrt{9\tan^2\phi + 8} + 3\tan\phi}, \beta_{cone,min}(\phi) = \beta(\phi, \gamma_*).$$

For fixed $0 < \beta_0 < 1$, the smaller-cone root between zero and γ_* exists precisely when $\beta_{cone,min}(\phi) \le \beta_0$. It continues from the radial-facing equatorial seed, assigning the same hardware different attitudes and angular rates at successive latitudes. Below the limiting latitude a second, larger-cone root exists; it approaches grazing incidence at the equator and does not continue the radial-facing seed. Appendix B gives the continuity argument and endpoint limits.

The minimum-lightness envelope increases monotonically from zero towards unity. A fixed $\beta_0 < 1$ therefore has a unique limiting latitude Φ_{max} satisfying

$$\beta_{cone,min}(\Phi_{max}) = \beta_0, \sigma_{lim}(\phi) = \frac{\sigma^*}{\beta_{cone,min}(\phi)}.$$

The outermost row at latitude Φ requires $\sigma_{sys} \le \sigma_{lim}(\Phi)$. Fig. 3 shows this local density limit across the full angular domain for a solar source. This is the local force-balance limit of the adopted ideal constant-latitude family, not a maximum instantaneous latitude for every orbit of the same hardware.

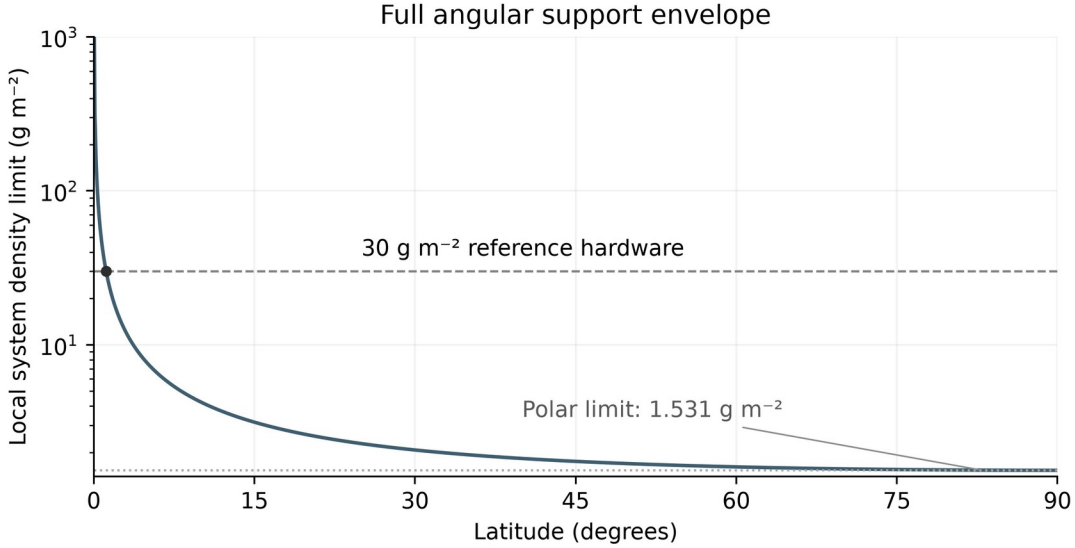


Fig. 3. Exact local support envelope for a solar source. The maximum supported system areal density decreases with latitude towards the polar limit. The horizontal reference at 30 g m^{-2} meets the curve near 1.158 degrees. The curve describes local support states with varying hardware requirements, not one finite swarm extending to the pole.

3.3 Full angular domain and radial scaling

The force law applies throughout $0 < \phi < 90^\circ$, with no small-latitude approximation. Latitude ϕ and cone angle γ are distinct variables satisfying $0 \le \gamma \le 90^\circ - \phi$. The one-degree construction in section 5 samples this general family with one fixed hardware class; it does not define the model's angular range.

The endpoints require separate interpretations. At the equator, a finite-mass radial-facing seed has $v^2 = 1 - \beta_0$; it is distinct from the zero-lightness equatorial limit of the optimised envelope. At exactly 90°, the latitude circle degenerates to a single axial point and angular rate no longer describes a distinct motion. Its ideal static support condition is $\gamma = 0$, $\beta = 1$.

At ordinary nonzero, nonpolar latitudes, statite states form the separate branch $\gamma = 0$, $\beta = 1$, $v = 0$. The optimised envelope varies the hardware requirement with latitude and does not become that statite branch. Its polar limit is distinct from continuation at fixed $\beta_0 < 1$; Appendix B gives the limiting kinematics.

The ideal support boundary is independent of stellar distance because both forces scale as r^{-2}. Moving unchanged hardware farther out changes angular rates and absolute clearances but does not remove its latitude limit. Higher lightness or a different support architecture is needed for broader coverage. Finite-size spacing imposes an additional requirement, developed next.

4. Finite-Size Compatibility

4.1 Reserved spacing at all relative phases

Analytic relative-distance bounds for more general displaced orbits have been developed by Wang et al. [12]. The common-radius, coaxial circles used here admit a simple all-phase bound that can be combined with finite-source visibility. To maintain clearance as rows rotate, the lattice reserves space up to a design half-width Φ_d. Choose a minimum centre separation d_0 and define

$$\delta = 2 \arcsin \frac{d_0}{2r}, \quad N = \left\lfloor \frac{\pi}{\arcsin\left[d_0 / \left(2r \cos \Phi_d \right) \right]} \right\rfloor .$$

The construction requires $N \ge 2$, $d_0 < 2r \cos \Phi_d$ and $J\delta \le \Phi_d < \pi / 2$. Adjacent centres in the same row are separated by at least

$$2r \cos \Phi_d \sin\left(\pi / N \right) \ge d_0 .$$

For different rows, minimising over their relative azimuth gives

$$|q_i - q_j| \geq \sqrt{(\rho_i - \rho_j)^2 + (z_i - z_j)^2} = 2r \sin\left(|\phi_i - \phi_j|/2\right) \geq d_0.$$

Consequently, the finite bounding balls remain disjoint whenever $d_0 > 2a$. The bound is independent of the phase relation between different rows. Reserving the azimuthal slot count using Φ_d prevents the circumference decrease at higher latitudes from eroding the specified spacing. The chosen geometry has its own reserved outer boundary, distinct from the force-law limit on accessible latitude.

4.2 A sufficient condition for direct illumination

Finite spacing can protect the illumination assumption throughout differential rotation. Let the stellar emitting region lie inside a ball of radius $R < r$. For two element centres on the common radius, the distance from either centre to any direct ray segment joining a stellar point to the other centre obeys

$$D \geq \frac{r - R}{2r} |q_i - q_j|.$$

Appendix A gives a geometric proof. Allowing both the receiving and potentially occulting elements their radius-a bounds yields the sufficient condition

$$d_0 > \frac{4ar}{r - R}.$$

Under this condition every ray from every stellar point to every point in a target element avoids all other bounding balls. It is stronger than the physical nonintersection condition and holds for all relative phases. Adding any subset of the reserved slots therefore leaves existing direct stellar illumination unobstructed.

This condition is sufficient, not necessary: violating it does not establish occultation. No optimal spacing or packing density is inferred.

4.3 Positive area and monotonic interception

For interception, take a central isotropic point source and count only direct first-pass light. For $0 < a < r$, a finite disc in the prescribed attitude subtends a strictly positive solid angle. If its centre is q, its normal is n and y is an in-plane displacement, then $n \cdot (q + y) = r \cos\gamma$. The exact solid angle is

$$\Omega = \int_A \frac{r \cos\gamma}{|q + y|^3} \, dA.$$

The bounds $r - a \leq |q + y| \leq r + a$ give

$$\frac{\pi a^2 r\cos\gamma}{(r+a)^3} \le \Omega \le \frac{\pi a^2 r\cos\gamma}{(r-a)^3}.$$

The non-occultation condition makes these direct-light footprints disjoint. For the completed rows of stage J, define

$$f_{0,J} = \frac{N a^2}{4r^2}\left(1 + 2\sum_{j=1}^{J}\cos\gamma_j\right).$$

The intercepted fraction of the source's total luminosity lies between $f_{0,J}(1+a/r)^{-3}$ and $f_{0,J}(1-a/r)^{-3}$. Each additional occupied slot adds positive solid angle without subtracting any previous direct contribution. This establishes monotonic interception for the finite construction, including partially populated new rows.

The outermost centres and the finite reflectors have slightly different containing bands. The centres extend to $J\delta$; their bounding balls fit inside a band of half-width $J\delta + \arcsin(a/r)$. Dividing interception by the latter band's solid-angle fraction gives a geometric projected filling fraction. Neither this ratio nor the intercepted stellar luminosity is an electrical conversion efficiency. Ideal specular reflectors redirect the intercepted radiation.

4.4 Nominal stage compatibility

Proposition 1 (Nominal stage compatibility). Choose $0 < \beta_0 < 1$ and a reserved lattice satisfying section 4.1, with finite reflectors and the model assumptions of section 2.2. For each occupied stage require

$$J\delta \le min(\Phi_d, \Phi_{max}), d_0 > \frac{4ar}{r-R}.$$

Assign its equatorial elements the seed state and its other elements the smaller-cone states from section 3. The geometry guarantees separated finite elements and unobstructed direct stellar rays for every occupied subset. For a central isotropic point source, each additional occupied slot contributes strictly positive direct first-pass interception through the finite-disc solid angle. The finite-source statement guarantees visibility without prescribing an extended source's radiance or intercepted fraction.

Under the independent-force assumptions of section 2.2, the earlier centre trajectories remain solutions of the same nominal equations when new slots are occupied, with their prescribed attitudes unchanged. This compatibility assumes point-source local radiation pressure and prescribed attitude tracking, with mutual gravity and secondary-reflection forces omitted. It establishes nominal compatibility without proving stability or transfers between stages.

The two width limits have different meanings. Φ_{max} is the hardware's local support boundary within the ideal constant-latitude family; Φ_d is the width for which this particular lattice reserves azimuthal clearance. The tighter of these two bounds limits the sequence.

5. A Worked Construction

5.1 Identical hardware from an equatorial ring to a belt

Consider the Sun at $r = 1$ astronomical unit, approximated here as 1.496×10^{11} m. The adopted solar luminosity and mass are 3.828×10^{26} W and 1.989×10^{30} kg. The calculation uses rounded constants $G = 6.674 \times 10^{-11}$ m³ kg⁻¹ s⁻² and $c = 2.998 \times 10^{8}$ m s⁻¹, giving $\sigma^{*} \simeq 1.530874$ g m⁻². These constants define the reproducible numerical example; displayed digits do not represent physical predictive accuracy. Let all systems have $\sigma_{sys} = 30$ g m⁻², so $\beta_0 = 0.05102913$. Choose a geometric node radius of 1 km, a centre pitch $d_0 = 6$ km and a reserved half-width of one degree. The finite-source illumination test uses $R = 6.957 \times 10^{8}$ m.

This prescription gives $N = 156636893$ slots per row and a latitude pitch of 4.010695×10^{-8} rad. Table 1 lists completed stages of the same reserved construction. Target widths are rounded labels: actual outer centre latitudes are the greatest integer multiples of the pitch below those labels. The local force equations are solved at those actual latitudes. Filling a new row does not require a change to an old row's cone angle, angular rate or initial phase.

Table 1. Successive stages for the same 30 g m⁻² system. The last column estimates the direct first-pass fraction of central-source luminosity; finite-disc bounds differ from the unrounded central-area estimates by less than 2.1×10^{-8} *fractionally.*

Target half-width	Rows	Outer γ	Outer ν	$f_{0,J}$
0°	1	0°	0.974151	1.74973×10^{-9}
0.25°	217585	4.68820°	0.974423	3.80293×10^{-4}
0.5°	435169	9.63321°	0.975280	7.57948×10^{-4}
1°	870337	22.69068°	0.979908	1.49005×10^{-3}

The completed one-degree stage contains approximately 1.36327×10^{14} elements. Its containing band spans approximately 1.745 per cent of the full solid angle. The reflectors occupy approximately 8.54 per cent of that band in projection, giving direct interception of about 0.1490 per cent of the stellar luminosity. This fraction describes the chosen conservative reserved lattice.

Packing has not been optimised, so it is not a maximum interception fraction for the hardware. The total assigned system mass is 1.28485×10^{19} kg. These quantities describe a geometric reference example. The assumed 30 g m^{-2} includes all supported mass; a structural design achieving this value for a kilometre-radius element has not been established.

5.2 Support margin and numerical accuracy

The same hardware's ideal constant-latitude support boundary is approximately 1.158°, while this lattice reserves slots only through one degree. Fig. 4 places the intercepted luminosity of the completed stages beside these separate boundaries. Continuing beyond the reserved width requires a new spacing check; a larger intended final width can instead be reserved at the outset with a smaller common slot count. The plotted connection between stages is a guide to the sequence, not a deployment timeline.

At one degree, $\beta_{cone,min} \simeq 0.0442473$, so $1 - \beta_{cone,min} / \beta_0 \simeq 0.133$. This is an equilibrium-existence margin allowing the nominal attitude and angular rate to be reselected, not a fixed-attitude error tolerance or a control margin. At Φ_{max} the two attitude roots merge and this margin vanishes; small force-model corrections can therefore move the limiting latitude.

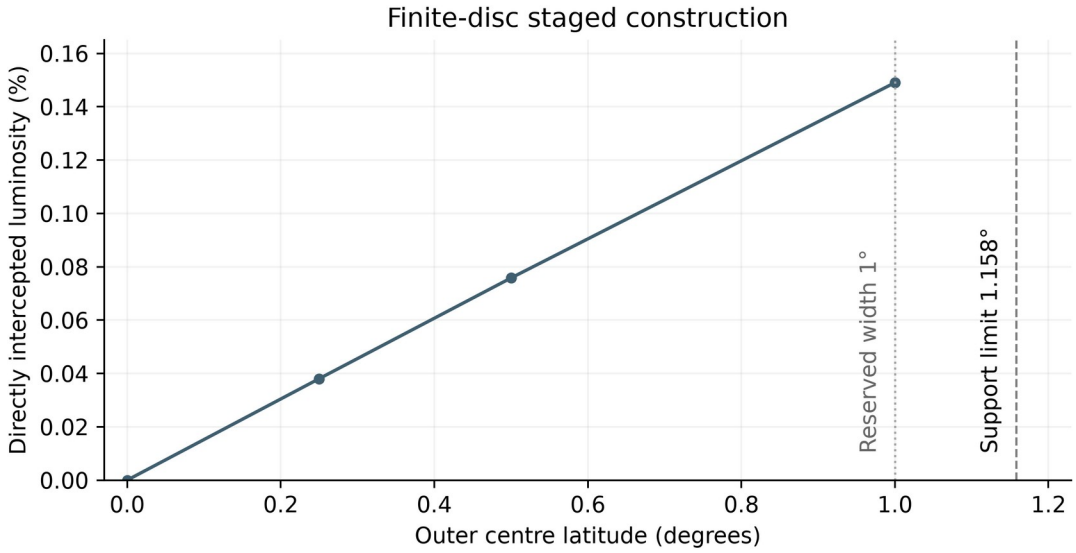


Fig. 4. Direct stellar interception in the fixed-hardware construction. Markers show the completed stages in Table 1. The reserved one-degree width and the hardware's 1.158-degree support limit are distinct. No stage beyond the reserved width is demonstrated. Interception is not electrical power.

The minimum physical gap between bounding balls is 4 km. The conservative lower bound on direct-ray clearance is 986.05 m, including the finite solar source. Both statements follow analytically from the lattice and illumination inequalities rather than from time sampling. Independent Cartesian

acceleration checks across all northern rows give a maximum dimensionless residual of 2.23×10^{-16}, with acceleration normalised by μ / r^2. Scalar evaluations of the existing single-sail model reproduce selected vectorised solutions to better than 2×10^{-16}. Random geometric probes additionally test the illumination inequality but do not replace its proof. These residuals check implementation consistency within the ideal model, not physical accuracy or stability.

The solar angular radius is about 0.266°, with $(R / r)^2 \simeq 2.16 \times 10^{-5}$, whereas $a / r \simeq 6.68 \times 10^{-9}$. For a uniform-brightness stellar disc at fixed radial energy flux and wholly in front of a non-grazing ideal sail, the leading finite-source force correction is second order in angular radius. This ideal-source scaling is distinct from the finite-reflector solid-angle bound in Table 1.

6. Discussion and Conclusion

The construction links supportable orbits to a sequence that accommodates finite collecting area. Its central geometric requirement is clearance at every relative phase: rows may rotate at different rates without losing physical separation or direct illumination. With prescribed attitudes and the independent-force assumptions, new slots can then be occupied without revising earlier nominal states.

Broader latitude extent imposes tighter mass requirements. A centre band spanning a fraction $f_{band} = \sin \Phi$ of the sky reaches $\Phi = 5.739^{\circ}$ at ten per cent extent and 30° at fifty per cent. The corresponding ideal solar outer-edge density limits are approximately 6.740 and 2.074 g m^{-2}. Towards the pole the limit approaches $\sigma^{*} \simeq 1.531$ g m^{-2}. These are total supported mass per reflector area; the containing band's angular extent is not an achieved interception fraction.

Radiation pressure supplies the axial force needed for nonzero-latitude circles at a common stellar distance. Ordinary Keplerian circles lie in planes through the star. Coplanar phase slots or separated radii also allow incremental construction. The present result concerns the additional geometry available with radiation assistance. Comparative mass, useful power and control cost are not evaluated here.

Preserving nominal geometry does not establish operational stability. A prescribed sail normal must be tracked, disturbances must be rejected and inserted elements must reach their allocated states. Coupled attitude–orbit dynamics and control require separate analysis [13]. Structural stresses, finite-aperture force variations, the extended-star radiation force, secondary reflections and mutual gravity require additional treatment. Failure-state

populations can behave very differently from their nominal orbit geometry, particularly in dense megaswarms [14]. The clearance result therefore does not imply a zero collision rate after failures or perturbations.

Within the ideal model, progressive growth can therefore be specified as a sequence of compatible nominal belts: choose the hardware, reserve spacing and add rows within both latitude limits. This establishes a self-consistent nominal path from a ring to a belt. It supplies a reference configuration whose separation and direct illumination are already characterised, allowing subsequent studies to examine how insertion, disturbances and failures affect those properties. The construction does not determine whether a civilisation would choose this architecture.

Appendix A. A Direct-Illumination Clearance Bound

Let $|q_i|=|q_j|=r$ and let a stellar emitting point satisfy $|s|\le R<r$. For a point $p=(1-t)s+t\,q_j$ on the centre-directed ray segment, convexity of the norm and the reverse triangle inequality give

$$D=|q_i-p|\ge r-|p|\ge(1-t)(r-R).$$

Also, $|p-q_j|\le(1-t)(r+R)$. Combining these inequalities yields

$$|q_i-q_j|\le D+|p-q_j|\le D\left(1+\frac{r+R}{r-R}\right)=\frac{2\,r\,D}{r-R}.$$

For a target point displaced by at most a from q_j, the corresponding ray point moves by at most $t\,a\le a$. The potentially occulting element extends at most another a from q_i. Its distance from every such ray is consequently at least $(r-R)\,d_0/(2r)-2\,a$. Positivity proves the stated sufficient no-occultation condition. The use of bounding balls makes the condition conservative and independent of individual disc orientations.

Appendix B. The Support Envelope and Its Endpoints

The minimum-lightness envelope follows by maximising $h(\gamma)=\cos^2\gamma\sin(\gamma+\phi)$ at fixed $0<\phi<\pi/2$. Its logarithmic derivative is

$$\frac{d\log h}{d\gamma}=\cot(\gamma+\phi)-2\tan\gamma.$$

This derivative decreases strictly from positive to negative across the admissible cone interval. The unique maximum satisfies $2t^2+3t\tan\phi-1=0$, where $t=\tan\gamma_*$. Its positive root gives the expression in section 3.2.

To compare with the original optimal halo mode, set $p=z/\rho=\tan\phi$ and $v=\Omega/\Omega_*$, where $\Omega_*^2=\mu/r^3$ and McInnes's sail angle α is γ. At the optimum, $v_*^2=(1+4t^2)/3$. Eliminating t gives

$$v_*^4-(2+3p^2)v_*^2+(1+p^2)=0.$$

This is McInnes's equation (4.13) divided by Ω_*^4 [5, p. 101]. The envelope is thus inherited; its use here selects the branch and latitude interval for identical hardware.

For $0<\beta_0<1$, the axial radiation force at $\gamma=0$ is below that required at nonzero latitude. It increases up to γ_*, so a smaller-cone solution exists exactly when the maximum reaches the required force. This solution is unique on the increasing branch and varies continuously until the limiting root merger. Near the equator it obeys $\gamma\simeq(\beta_0^{-1}-1)\phi$ and joins the fixed-hardware seed.

For fixed positive γ,

$$\frac{\partial\log\beta}{\partial\phi}=\cot\phi-\cot(\gamma+\phi)>0.$$

The admissible cone interval also shrinks as latitude increases. Since its minimum lies in the interior, these facts make $\beta_{cone,min}$ strictly increasing. Together with its endpoint limits they establish a unique Φ_{max} for each $0<\beta_0<1$.

The optimised envelope has equatorial limits $\beta_{cone,min}\to 0$, $\gamma_*\to\arctan(1/\sqrt{2})$ and $v\to 1$. These differ from continuing one fixed nonzero lightness to its radial-facing seed. At the polar boundary,

$$\phi\to 90^\circ:\gamma_*\to 0,\beta_{cone,min}\to 1,\sigma_{lim}\to\sigma^*,v\to 1/\sqrt{3}.$$

The nonzero limiting angular-rate ratio coexists with $\rho=r\cos\phi\to 0$ and tangential speed $\omega\rho\to 0$. Exactly at the pole the circular parametrisation degenerates. These limits do not identify the separate nonpolar statite branch.

Data and Code Availability

The accompanying supplementary file, KE_2026_10_15_reproducibility.zip, contains parameters, complete numerical constants, scripts, model source, stage tables, verification results and figure sources. Its manifest records software versions and source hashes, which identify the numerical inputs independently of the repository history. Versioned public releases are

available through the Zenodo record family at https://doi.org/10.5281/zenodo.19224635. The calculation computes row states without enumerating every element. Numerical probes supplement the analytic guarantees and do not constitute a long-term swarm simulation.

Acknowledgements and AI Assistance

OpenAI tools assisted with literature, derivation, numerical implementation, drafting and checks. Google Gemini assisted with narrative review. The author is responsible for source verification, scientific content and final conclusions.

References

[1] F.J. Dyson, “Search for artificial stellar sources of infrared radiation”, *Science*, 131, pp.1667–1668, 1960, doi: 10.1126/science.131.3414.1667

[2] J.T. Wright, “Dyson spheres”, *Serbian Astronomical Journal*, 200, pp.1–18, 2020, doi: 10.2298/SAJ2000001W

[3] R.G. Kennedy III, K.I. Roy and D.E. Fields, “Dyson Dots: Changing the solar constant to a variable with photovoltaic lightsails”, *Acta Astronautica*, 82, pp.225–237, 2013, doi: 10.1016/j.actaastro.2012.10.022

[4] U. Bhowmick and V. Khaire, “Yuti: A general-purpose transit simulator for arbitrary shaped objects orbiting stars”, *The Astronomical Journal*, 168, 243, 2024, doi: 10.3847/1538-3881/ad7d8d

[5] C.R. McInnes, *Advanced trajectories for solar sail spacecraft*, PhD thesis, University of Glasgow, 1991, https://theses.gla.ac.uk/78310/ (accessed 8 October 2026)

[6] C.R. McInnes and J.F.L. Simmons, “Solar sail halo orbits. Part I - heliocentric case”, *Journal of Spacecraft and Rockets*, 29, pp.466–471, 1992, doi: 10.2514/3.25487

[7] C.R. McInnes, “Dynamics, stability, and control of displaced non-Keplerian orbits”, *Journal of Guidance, Control, and Dynamics*, 21, pp.799–805, 1998, doi: 10.2514/2.4309

[8] C.R. McInnes, “Stellar engines and Dyson bubbles can be stable”, *Monthly Notices of the Royal Astronomical Society*, 546, stag100, 2026, doi: 10.1093/mnras/stag100

[9] S. Gong, H. Baoyin and J. Li, “Solar sail formation flying around displaced solar orbits”, *Journal of Guidance, Control, and Dynamics*, 30, pp.1148–1152, 2007, doi: 10.2514/1.24315

[10] C.R. McInnes and J.C. Brown, “The dynamics of solar sails with a non-point source of radiation pressure”, *Celestial Mechanics and Dynamical Astronomy*, 49, pp.249–264, 1990, doi: 10.1007/BF00049416

[11] V. Koblik, E. Polyakhova and L. Sokolov, “Solar sail near the Sun: Point-like and extended models of radiation source”, *Advances in Space Research*, 48, pp.1717–1739, 2011, doi: 10.1016/j.asr.2011.04.024

[12] W. Wang, J. Yuan, G. Mengali and A.A. Quarta, “Invariant manifold and bounds of relative motion between heliocentric displaced orbits”, *Journal of Guidance, Control, and Dynamics*, 39, pp.1764–1776, 2016, doi: 10.2514/1.G001751

[13] S. Gong, H. Baoyin and J. Li, “Coupled attitude–orbit dynamics and control for displaced solar orbits”, *Acta Astronautica*, 65, pp.730–737, 2009, doi: 10.1016/j.actaastro.2009.03.006

[14] B.C. Lacki, “Ground to dust: Collisional cascades and the fate of Kardashev II megaswarms”, *The Astrophysical Journal*, 985, 191, 2025, doi: 10.3847/1538-4357/adccc5